Pharm Res (2015) 32:1462–1474
DOI 10.1007/s11095-014-1552-7

RESEARCH PAPER

# Tunable CD44-Specific Cellular Retargeting with Hyaluronic Acid Nanoshells

Morten F Ebbesen • Morten TJ Olesen • Mikkel C Gjelstrup • Malgorzata M Pakula • Esben KU Larsen • Irene M Hansen • Pernille L Hansen • Jan Mollenhauer • Birgitte M Malle • Kenneth A Howard

Received: 23 June 2014 / Accepted: 10 October 2014 / Published online: 1 November 2014


## ABSTRACT

***Purpose*** In this work we specifically investigate the molecular weight (Mw) dependent combinatorial properties of hyaluronic acid (HA) for exhibiting stealth and targeting properties using different Mw HA nanoshells to tune nanoparticle retargeting to CD44-expressing cancer cells.

***Methods*** HA of different Mw was covalently grafted onto model polystyrene nanoparticles and advanced surface analysis by X-ray photoelectron spectroscopy performed to quantify and evaluate the effect of the coating procedure. Specific CD44-mediated retargeting was investigated by flow cytometry and confocal microscopy using isogenic D44-deficient and CD44-expressing MCF-7 breast adenocarcinoma cells.

***Results*** Surface analysis demonstrated effective surface coating with 33, 260 and 900 kDa HA resulting in increased colloidal stability and highly negative surface charge due to presentation of up to 4.7% carboxyl groups that indicates an extended and non-constricted HA polymer surface. Reduced non-specific particle interaction in $CD44^-$ cells was shown for all HA nanoshells but CD44-dependent cellular retargeting and internalization in $CD44^+$ cells was highly dependent on the coating HA Mw properties.

***Conclusion*** The combination of advanced surface characterization and evaluation of particle interactions in isogenic cells with and without CD44 receptor demonstrates direct evidence for the dual capacity of HA for stealth and CD44-mediated retargeting tunable by the HA molecular weight.

**KEY WORDS** Hyaluronic acid · stealth · targeting · cd44 · nanoparticles

## ABBREVIATIONS

| | |
|---|---|
| CDS | Coding DNA sequence |
| EDC | *N*-(3-Dimethylaminopropyl)-*N*-ethylcarbodiimide |
| HA | Hyaluronic acid |
| HMw | High molecular weight (900 kDa) |
| LMw | Low molecular weight (33 kDa) |
| MMw | Medium molecular weight (260 kDa) |
| MPS | Mononuclear phagocytic system |
| MWCO | Molecular weight cut-off |
| NHS | *N*-Hydroxysuccinimide |
| NTA | Nanoparticle tracking analysis |
| PEG | Poly(ethylene glycol) |
| P-blank | Noncoated nanoparticles |

**Electronic supplementary material** The online version of this article (doi:10.1007/s11095-014-1552-7) contains supplementary material, which is available to authorized users.

M. F. Ebbesen • M. T. Olesen • M. C. Gjelstrup • M. M. Pakula • I. M. Hansen • K. A. Howard
Interdisciplinary Nanoscience Center (iNANO), University of Aarhus
Gustav Wieds Vej 14, Building 1593, room 329, 8000 Aarhus, Denmark

M. F. Ebbesen • M. T. Olesen • M. C. Gjelstrup • M. M. Pakula • I. M. Hansen • K. A. Howard (✉)
Department of Molecular Biology and Genetics, University of Aarhus
8000 Aarhus, Denmark
e-mail: kenh@inano.au.dk

E. K. Larsen
Department of Micro- and Nanotechnology, Technical University of Denmark (DTU), 2800 Lyngby, Denmark

P. L. Hansen • J. Mollenhauer
Lundbeckfonden Center of Excellence NanoCAN, Institute of Molecular Medicine, University of Southern Denmark (SDU)
5000 Odense C, Denmark

P. L. Hansen
Small Animal PET Imaging Unit, Department of Nuclear Medicine, Clinical Institute, Odense University Hospital (OUH), 5000 Odense C, Denmark

B. M. Malle
R&D Technology Development, Novozymes A/S
2880 Bagsvaerd, Denmark

| | |
|---|---|
| P-HA33 | 33 kDa HA nanoshell |
| P-HA260 | 260 kDa HA nanoshell |
| P-HA900 | 900 kDa HA nanoshell |
| SEM | Scanning electron microscopy |
| TNBS | Trinitrobenzenesulfonic acid |
| XPS | X-ray photoelectron spectroscopy |

## INTRODUCTION

The effectiveness of a drug is dependent on reaching its target site at therapeutically relevant levels. Nanoparticle-based nanomedicines have been used for protection and improved delivery of bioactive agents (1,2). However, evasion of premature capture by the mononuclear phagocyte system (MPS), increasing the plasma circulatory half-life to accumulate and interact with the target site, termed retargeting, still remains a challenge to systemic particle-based drug delivery (3). Present strategies are based on two-component systems composed of a hydrophilic "stealth" material and targeting ligands (4) that constitute the surface or "nanoshells" when referring to the outermost nanoscale region. Poly(ethylene glycol) (PEG) (5) has been a promising strategy for controlling properties such as surface charge and hydrophilicity leading to low protein adsorption and reduced blood clearance (3). Its continued use and broad applicability, however, has been challenged by its non-biodegradable ether bonds, immunogenicity (6,7), and complement activation (8) particularly for high molecular weight (Mw) PEG (9). Importantly hydrophilic surface coatings, or nanoshells, do not by themselves confer active affinity towards tumor sites without construction of a hybrid particle containing targeting moieties. The inclusion of targeting moieties such as peptides or proteins, however, can induce immune responses that potentiate MPS capture if decorated onto the nanoparticle surface, whilst steric hindrance installed by the hydrophilic component can mask the recognition and consequent receptor engagement of the ligand. Attempts of ligand-based retargeting to receptor-bearing cells generally suffer from a poor balance between stealth and targeting due to these mutually compromising properties (10).

The outermost layer of a nanoparticle determines the biological interaction with plasma proteins, the MPS, and cellular membranes of the target cell. This "nanobio" interface can be modified by surface coatings or "nanoshells" that can be precisely investigated by advanced characterization tools, which is, however, rarely performed. A dual capacity for stealth properties and retargeting to specific cell types in a single well-characterized coating material would offer a novel approach in nanoparticle-based drug delivery.

Hyaluronic acid (HA) is a linear polysaccharide of the glycosaminoglycan type. Its size varies from 5 kDa to 10 MDa *in vivo*, and it consists of disaccharide repeating units of glucuronic acid and *N*-acetyl glucosamine linked by alternate β1-3 and β1-4 linkages (11). HA is ubiquitously present in the body and, in contrast to PEG, is both biodegradable and biocompatible (12). The polysaccharide exists in solution as a slightly stiffened, but highly flexible random coil attributed to its linear chain conformation and ability for hydrogen bonding to water (13). This and its negative charge provided by carboxyl groups contributes to both steric and electrostatic hindrance of cell interactions as a liposome coating that has been investigated by Peer *et al.* (14).

CD44 is a cellular surface receptor involved in cell proliferation, differentiation and migration as well as in signaling for cell survival (15). These properties are also associated with the pathological activities of cancer cells and CD44 has been shown both to control and to be upregulated in a range of human cancers such as melanomas (16), multiple myeloma, breast carcinoma and squamous cell carcinomas (17,18). The CD44 receptor has been suggested to engage with HA with a Mw dependency (19,20) and has been used as a target for HA functionalized nanomedicines such as liposomes (21,22) or polyplexes (23). Previous studies, however, use different cell types exhibiting different CD44 receptor levels for evaluating CD44-dependent cellular uptake (22). By the use of isogenic cell lines we intend to provide a clearer picture of the HA-CD44 interaction without possible interference from cell type or genetic/molecular differences enabling a precise investigation of the combined capability of HA coatings to confer both stealth properties and CD44-mediated nanoparticle retargeting.

In this work advanced surface analysis is performed to characterize the outmost 10 nm surface of model latex 200 nm nanoparticles coated with different Mw HA enabling precise interpretation of the effect of a particular coat on the biological performance. Furthermore, the capability of HA "nanoshells" to install a dual stealth and CD44-mediated retargeting capacity to fluorescent nanoparticles (Fig. 1), tuned by HA Mw, is investigated using flow cytometry and confocal microscopic analysis in isogenic MCF-7 breast adenocarcinoma cell lines engineered either for absence ($CD44^-$) or high ($CD44^+$) CD44 expression to limit any influence due to intrinsic differences between different cell types or expression of HA receptors other than CD44.

## MATERIALS AND METHODS

### Materials

Hyaluronic acid of 33, 260 and 900 kDa (referred in the text as low LMw, medium MMw and high HMw, respectively) were supplied by Novozymes Biopharma DK A/S (Denmark). The experimental samples of 33 and 260 kDa were prepared by well-controlled hydrolysis of HA material

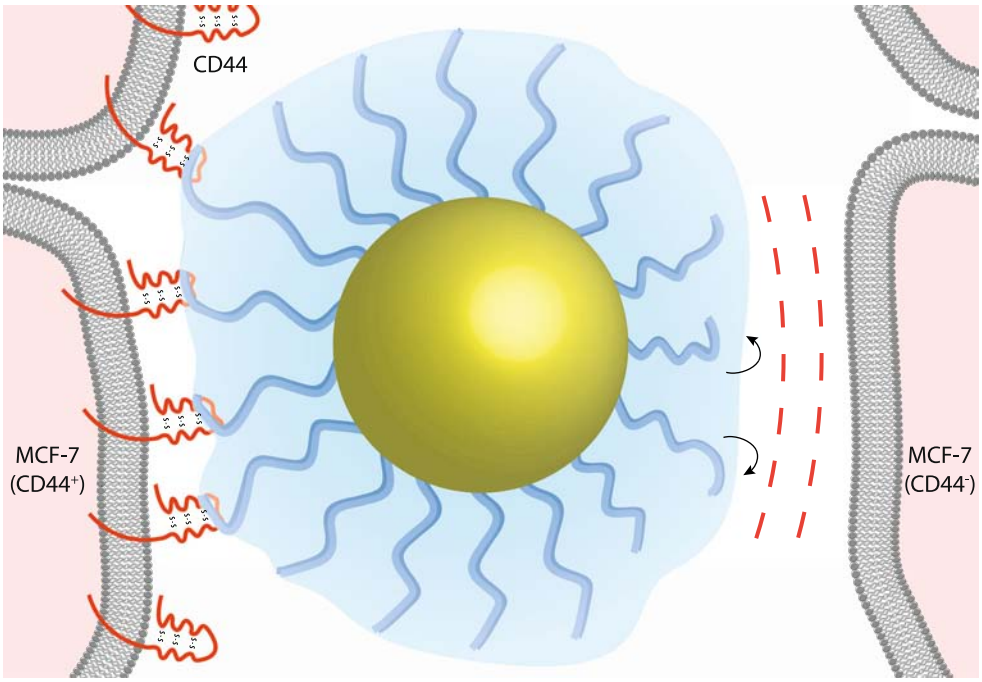


**Fig. 1** Schematic representation of the dual capacity of hyaluronic acid (HA) for both stealth and CD44-targeting. HA confers steric hindrance to unspecific cellular adhesion in CD44 negative MCF-7 cells (*right*) but retargeting to CD44 positive MCF-7 cells (*left*).

with Mw of 900 kDa (24). The weight average Mw ($M_w$) and the Mw distribution ($M_w/M_n$) was determined by size-exclusion chromatography with online multiangle laser light scattering and refractive index detection. $M_w/M_n$ ranged from 1.3 to 1.7 for the LMw and MMw samples whereas the HMw sample had a $M_w/M_n$ of 1.4. A CD44-negative MCF-7 cell line was derived from the original MCF-7 cell line (obtained from ATCC) via subcloning after stable insertion of a sequence suitable for subsequent Flp-recombinase-mediated insertion of expression plasmids. The cell line was used to insert the coding sequence (CDS) of the standard variant of CD44, known as CD44S or CD44 isoform 4 (NM_001001391.1; Consensus CDS CCDS31457.1) under the control of a constitutive cytomegalovirus promoter, which yielded the $CD44^+$ cells. In parallel, the empty expression plasmid was inserted via Flp-mediated site-specific recombination into the same parental cell line to obtain isogenic $CD44^-$ MCF-7 cells. The $CD44^-$ and $CD44^+$ status of the isogenic cell line pair was confirmed by quantitative reverse transcription PCR, using TaqMan™ assays specific for CD44 and allowing for detection of all CD44 variants, by flow cytometry and by Western blotting using CD44-specific antibodies. Fluorescent (505/515, ex/em) FluoSpheres amine-modified 200 nm particles, DMEM glutamax, hygromycin B, Alexa 647 modified goat anti-mouse antibody, penicillin and streptomycin were purchased from Life Technologies Europe. Protease inhibitor cocktail was purchased from Roche. Mouse anti-human CD44 antibody was purchased from Thermo Scientific. BSA, Dako fluorescent mounting medium, Dulbeccos PBS, ethylene diamine, foetal bovine serum (FBS), insulin, propidium iodide, 2-(N-Morpholino)ethanesulfonic acid hydrate (MES), $NaN_3$, N-Hydroxysuccinimide (NHS), N-(3-Dimethylaminopropyl)-N′-ethylcarbodiimide (EDC), Sodium tetraborate decahydrate, Trinitrobenzenesulfonic acid (TNBS) solution 5% w/v in $H_2O$ and Hoechst nucleus stain were purchased from Sigma Aldrich (USA). Ultrapure water (Siemens Ultra Clear Basic plus) was used in all experiments.

## HA Coating of Nanoparticles

HA nanoshells were produced by grafting HA (33, 260 and 900 kDa) onto aminated polystyrene nanoparticle surfaces referred to as P-HA33, P-HA260 and P-HA900 respectively, by EDC/NHS activated covalent coupling. Prior to coupling the particles were washed with water by the use of sonication and vivaspin 2 concentrators (molecular weight cut-off, MWCO 0.2 μm) to remove surfactants from the stock solution. The surface amine concentration on the particles was measured using a trinitrobenzenesulfonic acid (TNBS) assay. Briefly, nanoparticles (50 uL, 2.0 wt%) or water (control) were diluted 1:4 into borate buffer (50 mM, pH 9.0) containing double the concentration of TNBS as the expected amine concentration. After stirring for 2 h at 37°C and centrifugation at 20,000*g* for 10 min, the supernatant was collected and the non-reacted TNBS reacted with ethylene diamine in excess. TNBS absorbance (421 nm) was used for calculating the amine surface concentration by subtracting the residual TNBS amount in the supernatant from the non-reacted TNBS control, resulting in an amine concentration of $1.4 \cdot 10^{-5}$ M for the nanoparticle dispersion corresponding to a nanoparticle surface amine density of 1 group per 69 $nm^2$. HA

(33, 260 and 900 kDa) was dissolved in MES buffer (50 mM, pH 6) and mixed with EDC/NHS (20 eq. to HA COOH). Nanoparticles were sonicated for 2 min and the HA/EDC/NHS solution was added to a magnetically stirred dispersion of nanoparticles (0.48 mg) (excess HA COOH groups with ~1 HA polymer molecule per particle surface amine) in MES buffer, in a flat bottomed plastic tube in a total volume of 0.6 ml. After reacting 20 h at 25°C, the nanoparticles were collected, washed thoroughly with water using vivaspin 2 concentrators (MWCO 0.2 μm) and the dispersion kept at 4°C.

## X-ray Photoelectron Spectroscopy for Determination of Surface Coated HA

Samples for X-ray photoelectron spectroscopy (XPS) were prepared by drying particles (~1 mg) on a clean aluminum XPS sample holder. XPS was performed on a K-Alpha spectrometer (Thermo Fisher Scientific, UK) using a 400-μm wide monochromatized Al Kα X-ray spot and collection of the emitted photoelectrons at a take-off angle of 0° to the surface normal. Charge compensation was used on all samples. High resolution scans were obtained with a pass energy of 50 eV and analyzed using CasaXPS version 2.3.15 for determination of C1s functional group (aromatic C-H at 284.8 eV, C-C/C-H at 285.0 eV, C-O-C/C-OH, C-N and O-C-C(O) at 286.3 eV, N-C=O and O-C-O at 287.6 eV and C(O)O at 289.0 eV, see Fig. 2) composition on the nanoparticle surface. The constraints used for fitting were +/- 0.1 eV for component binding energy positions and in general a maximum full width at half maximum (FWHM) of 1.5 eV for C1s components covering more than one carbon species and of 1.3 eV for those covering one species. Shirley background subtraction was used for all spectra.

## Evaluation of Nanoparticle Surface Charge, Size and Morphology

Zeta potential was measured in triplicates with a Zetasizer Nano ZS (Malvern, Worcestershire, UK) by diluting the particles 1:50 in $PO_4^{3-}$ buffer (20 mM, pH 7.5) and measuring at 25°C (Table I). Nanoparticle scattering spectras of 60 s were captured on a NanoSight LM10-HS (NanoSight Limited, Amesbury, U.K.) equipped with a sample chamber with a 405-nm laser and analyzed with Nanoparticle Tracking Analysis (NTA) software, version 2.3 to measure the particle hydrodynamic size distribution. Samples were diluted to obtain a suitable concentration of ~$6.0\times10^8$ nanoparticles $ml^{-1}$ in a phosphate buffer (pH 7.5) at 23°C. The NTA graphs are averages of three measurements. For the Scanning Electron Microscopy (SEM) imaging, particles were air-dried onto aluminum stubs (Electron Microscopy Sciences) and subsequently sputter coated with gold (1.25 kV, 1.5 min). SEM analysis was performed using a NOVASEM in high vacuum mode.

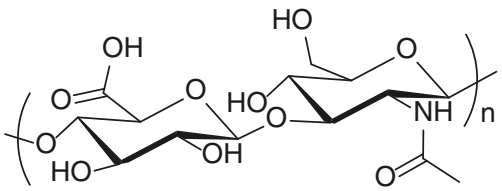


**Fig. 2** Hyaluronic acid disaccharide repeating unit ($n$=[3; ~26,000]) of glucuronic acid and N-acetyl glucosamine linked by alternate β1-3 and β1-4 linkages.

## Flow Cytometric Analysis of Cellular Nanoparticle Uptake and Cell Viability

Fluorescent nanoparticle dispersions had approximate concentrations of $6.0\times10^{11}$ particles $ml^{-1}$ as measured by NTA. The particle concentration in individual dispersions were more accurately determined based on the absorbance of the dye (yellow-green dye, ex/em 505/515 nm) isolated from the nanoparticles by drying 50 uL aliquots of nanoparticle dispersion and redissolving in chloroform to measure the dye-related absorbance at 515 nm. Absorbance levels were the basis for ensuring the addition of a uniform level of fluorescent particles to cells for the different particle types (supporting online information, Fig. S1).

Cellular uptake studies were performed in MCF-7 human breast adenocarcinoma cell lines that were engineered to differ in the presence/absence of CD44 but otherwise were genetically identical, *i.e.* isogenic cell lines (see details in the Materials section). The isogenic cell lines allowed analyzing nanoparticle properties solely depending on the presence/absence of the cognate receptor CD44, eliminating effects of other cell surface molecules and effects that might be contributed by differential uptake efficacies that may depend on cell type or genetic/molecular differences. Cells were maintained at 37°C with 5% $CO_2$ in MCF-7 media composed of DMEM Glutamax medium supplemented with foetal bovine serum (10%), Streptomycin (100 μg $ml^{-1}$), Penicillin (100 units $ml^{-1}$), Insulin (10 μg $ml^{-1}$), and from the fourth day post resuscitation the MCF-7 media was additionally supplemented with hygromycin (120 μg $ml^{-1}$). Cells were passaged minimum three times before use and when 70 – 80% confluent with a subcultivation ratio at 1:3 – 1:10. Cells were seeded at concentrations of $2.5\times10^5$ cells/well in 1 ml medium in a 24-well plate. 24 h later the medium was replaced with medium (250 μL) containing nanoparticles adjusted to a uniform concentration of approximately 50 particles/cell seeded. After 24 h the medium was removed followed by 2 x PBS wash and the cells harvested by trypsin treatment and centrifuged at 300 g for 5 min. Following an additional PBS wash, cells were resuspended in sterile-filtrated PBS flowbuffer (0.5 ml)

**Table I** Nanoparticle Surface Characterization; X-ray Photoelectron Spectroscopy (XPS) Analysis and Zeta Potential (in 20 mM pH7.5 $PO_4^{3-}$ Buffer) of Relevant Constituents and Different Coated Nanoparticles

| | XPS C1s spectra composition [%[ | | | | | Zeta potential [mV] |
|---|---|---|---|---|---|---|
| | 289.0 | 287.6 | 286.3 | 285.0 | 284.8 | $PO_4^{3-}$ 20 mM, pH 7.5 |
| A) Constituents | | | | | | |
| HA (calc.) | 7.1 | 21.4 | 57.1 | 14.3 | 0.0 | N/A |
| P-blank | 1.4 (±0.1) | 9.2 (±1.0) | 32.1 (±0.7) | 14.2 (±0.4) | 43.1 (±1.4) | −8.7 (±1.3) |
| B) HA coated particles | | | | | | |
| P-HA33 | 1.7 (±0.0) | 8.8 (±0.7) | 32.6 (±1.7) | 14.2 (±0.6) | 42.8 (±1.7) | −36.4 (±2.6) |
| P-HA260 | 2.3 (±0.2) | 10.6 (±0.5) | 29.9 (±0.9) | 14.2 (±0.5) | 43.0 (±1.0) | −42.5 (±3.3) |
| P-HA900 | 4.7 (±0.2) | 12.2 (±0.8) | 40.5 (±1.4) | 14.4 (±0.3) | 28.2 (±1.8) | −48.3 (±2.1) |

The average of three measurements is displayed and standard deviation given in brackets

containing BSA (1%) and $NaN_3$ (0.1%). Propidium iodide (1 μg $ml^{-1}$) was included to stain for cells with low viability and heat treated (60°C for 2 min) cells provided a low viability control.

Cellular uptake studies using pre-incubation with an increasing concentration of free HA was performed to quantitatively assess the specificity of the CD44 HA interaction. Maintenance and seeding of the MCF-7 ($CD44^+$ only) cell line was performed as described above for the regular uptake study. The cells were pre-incubated with HA of either 33 kDa or 900 kDa in a concentration range of 0.00, 0.01, 0.10 and 5.00 mg/mL in medium (250 μL) for 1 h and the HA containing media removed prior to a 3 h incubation with particles (~50 particles/cell) in serum free media (250 μL). Hereafter the cells where harvested as in the regular uptake study. PS-blank was not included in this part of the analysis due to interactions between the negatively charged free HA and the uncoated and partly cationic ($-NH_3^+$) particle surface.

For both types of uptake studies, flow cytometry was performed using a Gallios (Beckman Coulter) flow cytometer using a 488 nm laser and the 525/40 nm filter (FL1) for nanoparticle associated fluorescence and the 620/30 nm filter (FL3) for propidium iodide fluorescence detection of dead cells. A minimum of 10,000 events were collected for each sample and flow cytometric data analyzed using the Kaluza 1.2 software. The compensation matrix was adjusted to account for fluorescence spectral overlap of FL1 and FL3. Cell population selection was based on forward and side scattering, and was gated to distinguish dead cells and cell doublets. For the regular uptake study, the average value of three replicates of the geometric mean value of the FL1 channel histogram was used for quantification of nanoparticle uptake. Averages were normalized to $CD44^-$ cells treated with non-coated nanoparticles (P-blank). For quantifying the competitive binding effects from free HA, the FL1 channel histogram was first gated to determine the percentage of cells showing particle uptake compared to the total cell population (fluorescent and non-fluorescent cells, supporting online information, Fig. S2). The average percent-value of three replicates was then normalized to the value for 0.00 mg/mL free HA pre-incubation and uptake changes due to free HA pre-incubation depicted as deviations from 0% (no change in uptake). Statistical changes in both uptake studies were calculated using Students *t*-test. A "p" value less than 0.05 was considered statistically significant.

## Western Blot Detection of Cellular CD44

The expression levels of CD44 were verified by Western blotting. $1\times10^6$ MCF-7 cells were lysed in RIPA buffer (1x PBS, 1% NP-40, 5 mg/ml SDC, 0.1% SDS, 1x Protease inhibitor cocktail) and total protein extract (30 μg) was loaded and separated by 10% SDS-PAGE in X-Cell SureLock™ Mini-Cell chamber (Invitrogen) for 1.5 h at 110 V. Page Ruler™ Prestained Protein Ladder (Fermentas) was used as a size marker. Electrotransfer to Immobilon-P PVDF (Millipore, 0.45 μm) membrane was performed using X-Cell II™ Blot Module (Invitrogen) in 1x Transfer Buffer (0.3% Trizma base, 1.44% Glycine, 20% EtOH (96%)), 25 V for 2 h in 4°C. The membrane was activated in 96 ethanol for 30 s, followed by a 3 min water wash. Proteins were then visualized using Ponceau Red (0.5%) in acidic acid (5%) to confirm transfer and equal loading. The membrane was blocked with blocking buffer (5% milk in PBS-Tween 0.05%) for 1 h at RT, followed by mouse anti-human CD44 primary antibody (1ug $ml^{-1}$) incubation in blocking buffer at 4°C overnight. After washing in PBS-Tween (0.005%), the membrane was incubated with HRP conjugated goat anti-mouse secondary antibody (1ug $ml^{-1}$) in blocking buffer for 1 h at RT. Blots were developed using an ECL Plus kit (GE Healthcare), exposed in the dark on X-ray film.

## CD44-mediated Cellular Uptake Using Confocal Microscopy

Presentation of the CD44 receptor and receptor specific uptake was investigated using fluorescent antibody labeling and

confocal laser scanning microscopy. MCF-7 cells (either $CD44^+$ and $CD44^-$) were seeded in 8 well tissue culture chamber slides (Sarstedt, Germany) at a density of $2.5\times10^4$ cells/well in MCD-7 media (0.5 ml) for 24 h. Cells were then incubated with either P-HA260, P-HA900 or P-blank control nanoparticles for 24 h with subsequently removal of particles and wash. Cells were fixed for 10 min with 10% of formalin, washed and permeabilized using Triton X-100 (0.1%) for 30 min and washed and blocked with BSA (3%) in PBS for 30 min. The cells were then incubated at 4°C overnight with a mouse anti-human CD44 primary antibody (diluted to 4.7 μg $ml^{-1}$ in 3% BSA in PBS), washed thoroughly and subsequently incubated with an Alexa 647 goat anti-mouse secondary antibody (diluted to 4 μg $ml^{-1}$ in 3% BSA in PBS) for 1 h at room temperature in the dark. The nucleus was counter-stained with Hoechst. After 3 additional washes the cells were mounted with fluorescence mounting medium under a coverglass and sealed with nail polish and imaged using confocal laser scanning microscopy (LSM 710, Carl-Zeiss Inc., Thornwood, NY).

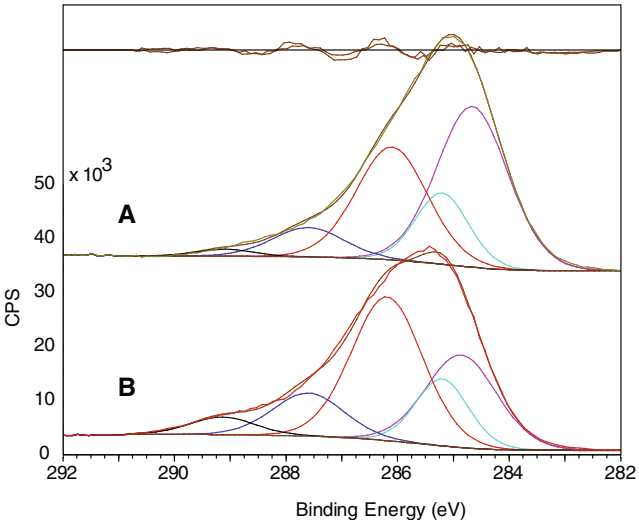


**Fig. 3** Decomposed X-ray photoelectron spectroscopy (XPS) C1s spectrum of (**a**) uncoated particles or (**b**) particles with HA nanoshells of 900 kDa. The five C1s components are aromatic C-H at 284.8 eV, C-C/C-H at 285.0 eV, C-O-C/C-OH, C-N and O-C-C(O) at 286.3 eV, N-C=O and O-C-O at 287.6 eV and C(O)O at 289.0 eV.

## RESULTS

### Physicochemical Characterization of HA Coated Nanoparticles

XPS analysis revealed the detailed chemical state information in the C1s spectra, revealing the changing particle surface chemistries. Analysis was performed by curve-fitting the C1s spectra into five peaks containing each a number of functional groups: Aromatic C-H (styrene) at 284.8 eV, C-C/C-H at 285.0 eV, C-O-C/C-OH, C-N and O-C-C(O) at 286.3 eV, N-C=O and O-C-O at 287.6 eV and C(O)O at 289.0 eV) (Fig. 3 and Table I). The C1s chemical species composition of the constituents (Table Ia), shows the spectra composition profile change from an unmodified particle surface (P-blank) to pure HA polymer (calculated from the HA disaccharide unit structure, Fig. 2). An increase in the Mw of HA (Table Ib), resulted in a composition profile change towards that for pure HA. As unmodified particle surfaces contained low amounts of C(O)O components such as carboxylic acid, a direct quantification of the surface-grafted HA amount could be based on the C1s level of the C(O)O component. This component increased from 1.4% (P-blank) to 1.7 2.3% and 4.7% for the HA nanoshells (P-HA33,−260 and−900 samples, respectively) reflecting the change in the dry state HA surface amount and the hydrated thickness due to the higher Mw of the P-HA900 nanoshell.

Zeta (ζ) potential is the electric potential originating from charged species ($-NH_3^+$, $-COO^-$, $-SO_3^-$ *etc.*) measured a few nanometers distance away from the particle surface. As a standard method to evaluate the surface functionalization of HA coated particles, ζ-potentials were measured in a 20 mM pH 7.5 $PO_4^{3-}$ buffer (Table Ia-b). Uncoated surfaces (P-blank) displayed a net ζ-potential of−8.7 mV at this pH-value indicating the presence of mixed charged species, while negative ζ-potentials (−36.4,−42.5 and−48.3 for P-HA33,−260 and −900 samples, respectively) indicated a major presence of $COO^-$ groups from HA surface conjugation. Control experiments utilized ζ-potential measurements for confirmation of covalent surface conjugation of HA by comparing coatings performed with and without the addition of EDC/NHS reagents. Particles mixed with HA (33 kDa) without EDC/NHS and purified had a slightly lower ζ-potential (−14.2 mV, data not shown in Table I) compared to P-blank (−8.7 mV). A substantially lower surface charge (−36.4 mV) for particles coated with HA using EDC/NHS, strongly indicated covalent attachment of HA.

Nanoparticle Tracking Analysis (NTA) (Fig. 4) was used to measure the particle hydrodynamic size distribution in an aqueous environment and SEM (Fig. 5) to evaluate the dry state morphology of the particles. NTA showed that samples of HA coated particles (P-HA33,−260 and−900) had a narrow size distribution profile around 200 nm, with P-HA33 being closest to 200 nm. Inherent hydrophobic nanoparticles without nanoshells (P-blank) had an apparent broader size distribution with discrete peaks of 200 nm distance that indicates small aggregates consisting of 2–5 uncoated particles.

SEM analysis (Fig. 5) showed highly uniform, discrete and spherical particles of 200 nm in diameter, which correlated with the hydrodynamic particle size of HA coated particles determined by NTA. Coating with HA nanoshells of different Mw (Fig. 5b-d) did not visibly affect the dry state size of the

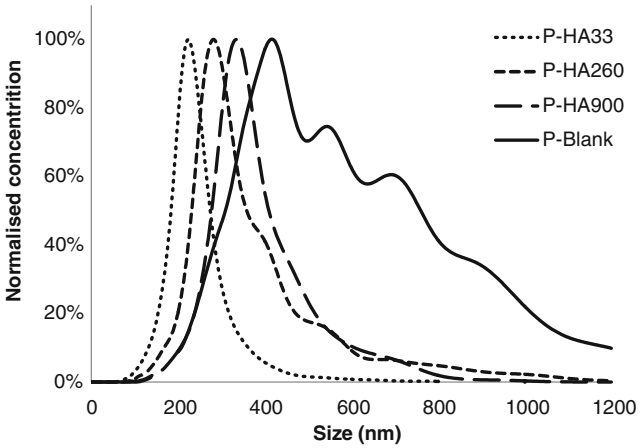


**Fig. 4** Nanoparticle Tracking Analysis (NTA), showing the hydrodynamic size distribution of hyaluronic acid (HA) coated particles resuspended in 50 mM phosphate buffer pH 7.5. Distributions are averages of three measurements. Standard deviations are omitted for clarity.

individual particles, but had an influence on the dispersion drying process, especially for the 900 kDa HA nanoshells (Fig. 5d); first to induce a degree of interparticle ordering into a hexagonal arrangement as sketched in Fig. 5e, and secondly to reduce the number of overlapping particles.

## CD44-mediated Cellular Retargeting

Cellular uptake studies were performed in MCF−7 cells that were genetically identical (isogenic) except for the CD44 status and derived as described in the Materials section via a modified site-specific Flp-mediated recombination system. The $CD44^-$ and $CD44^+$ status was confirmed via Western blotting (Fig. 6 insert and supporting online information, Fig. S3). The use of isogenic cell lines allowed eliminating all differences that might be caused by cell type or genetic/molecular changes, so that both the stealth properties and the specific CD44-targeting could be addressed without interference from other factors. The uncoated and inherently hydrophobic polymer nanoparticles displayed substantial unspecific uptake in both $CD44^-$ and $CD44^+$ cells (Figs. 6 and 7), which was used as reference point (Fig. 6). Coating with any of the three HA types reduced unspecific uptake (66%, 73% and 73% reduction, $p<0.01$) close to the background value of the cells autofluorescence, as indicated by the data obtained for the $CD44^-$ cells, however, with slightly improved properties for P-HA260 and P-HA900 compared to P-HA33 (7% lower uptake, $p<0.01$). The data indicated that all three HA types highly efficiently prevented the nanoparticles from unspecific uptake, supporting a shielding function. Remarkably, P-HA260 and P-HA900 dramatically promoted specific, *i.e.* CD44-mediated, retargeting (Fig. 6) as demonstrated by the fluorescence levels of the isogenic $CD44^+$ cells being much higher than cells without the CD44 receptor ($CD44^-$) (64% increase, $p<0.01$ for P-HA260 and 67% increase, $p<0.01$ for P-HA900, when comparing $CD44^+$ to $CD44^-$ cells). P-HA33 nanoshells exhibited only minor uptake enhancement (6%, $p<0.01$, comparing $CD44^+$ to $CD44^-$ cells) indicating a lower CD44-HA affinity. Measurement of propidium iodide fluorescence indicated a low level of membrane damage and further confirmed that all four kinds of nanoparticles were not toxic to the cells (supporting online information, Fig. S4).

To further confirm CD44 specificity and for a more quantitative analysis of the CD44-HA interaction a competitive binding analysis was performed by pre-incubating CD44 positive MCF-7 cells with free HA of 33 and 900 in a concentration range from 0.0 to 5 mg/mL before the addition of particles to the cells. For P-HA33 nanoshells the pre-incubation with 33 kDa free HA up to 5 mg/mL did not significantly change the cellular particle uptake (3.4%, $p=0.37$) (Fig. 8a) whereas a significant but small change was seen for 900 kDa free HA (20% reduction, $p<0.01$) (Fig. 8b). Cellular uptake of PS-HA260 and PS-HA900 was clearly affected by the pre-incubation with free HA with a 42% (PS-HA260) and 46% (PS-HA900) ($p<0.01$) decrease in cellular uptake for 33 kDa free HA and an almost complete inhibition of uptake (PS-HA260 and PS-HA900 both reduced by 85%, $p<0.01$) by 900 kDa free HA at 5 mg/mL. Generally, more cellular uptake reduction was observed for free HA with a Mw of 900 kDa (Fig. 8b) compared to 33 kDa (Fig. 8a) (17% to 43% larger at 5 mg/mL, $p<0.02$). For all concentrations of free HA, no signs of toxicity was shown in this part of the study.

Immunostaining of the MCF-7 ($CD44^+$ and $CD44^-$) cells with anti-human CD44 antibodies and confocal microscopic analysis demonstrated a clear presence of the CD44 receptor on the cell surfaces for the $CD44^+$ cells and absence of CD44 on the $CD44^-$ cells (Fig. 7), which confirmed the Western blot studies (Fig. 6, insert). P-HA260 and P-HA900, that showed both effective shielding and CD44-dependent interaction according to the flow cytometry results, were analyzed in further detail with confocal microscopy for visualization of the CD44 involvement and the intra/extracellular localization of HA coated nanoparticles. Unmodified particles (P-blank), showed non-specific cellular interaction with both $CD44^+$ and $CD44^-$ cells, as revealed by green dots surrounding the cellular membranes (Fig. 7, P-blank, $CD44^{+/-}$), supporting the flow cytometry results. Nanoparticles P-HA260 and P-HA900 were only observed within the $CD44^+$ cells, especially in areas of high CD44 expression, suggesting effective shielding against non-specific cellular interactions ($CD44^-$) and successful retargeting and internalization through CD44-HA interaction with these coatings in agreement with the flow cytometry data (Fig. 6).

## DISCUSSION

In this work we investigate the ability of hyaluronic acid coatings of different Mws to introduce a hydrophilic HA

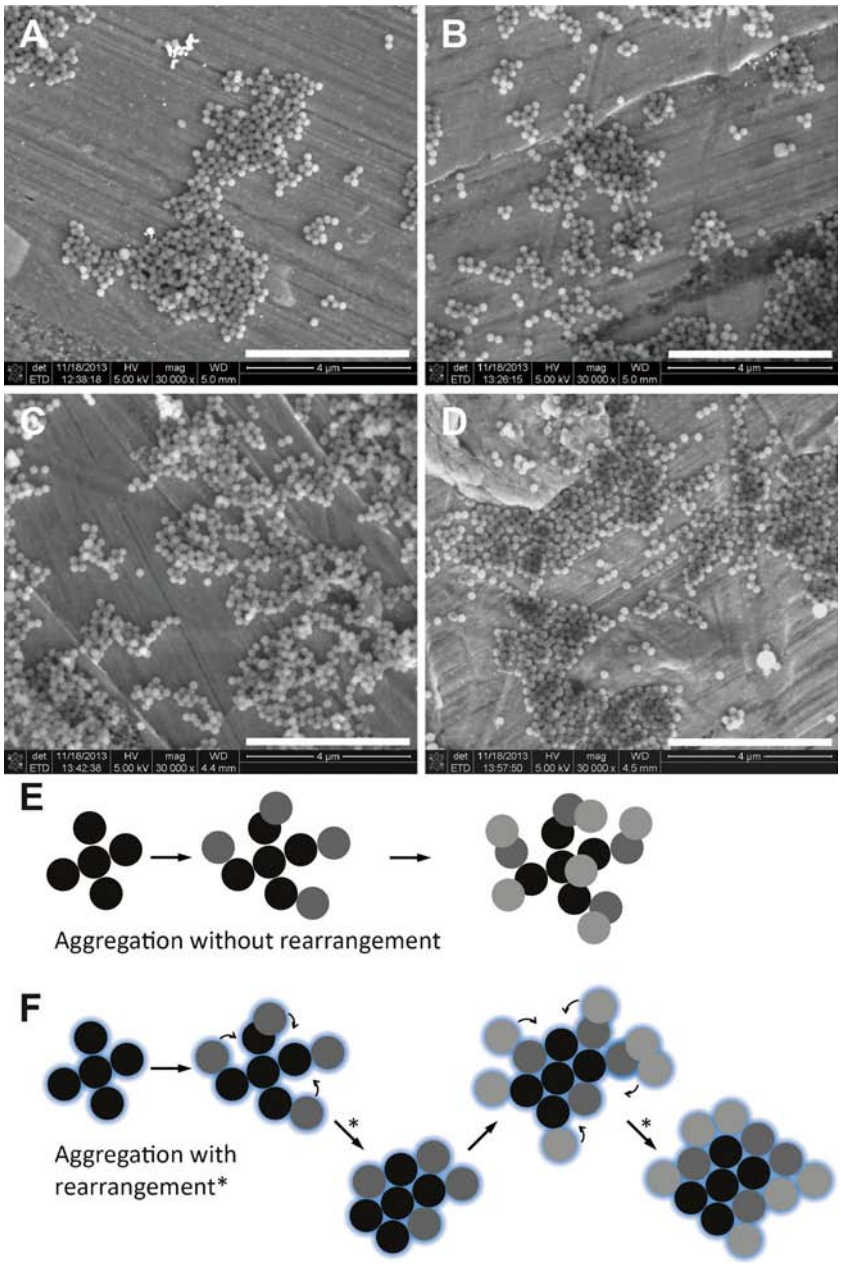


**Fig. 5** A-D: Scanning Electron Microscopy (SEM) images of uncoated particles (**a**) and particles with 33, 260 and 900 kDa HA nanoshells (**b**-**d**). Particles were all spherical and uniform of 200 nm. HA nanoshells of especially 900 kDa HA induced a degree of hexagonal ordering, indicating highly uniform coatings. Particles were resuspended in water, deposited onto aluminum SEM stubs and dried before SEM analysis. Bar on image corresponds to 4 $\mu$m. (**e**)-(**f**): Schematic showing aggregation without rearrangement of particles without HA coating (**e**) and with rearrangement for 900 kDa HA coated particles (**f**).

nanoshell for cellular CD44-specific retargeting of model polystyrene nanoparticles. We utilize advanced surface characterization including XPS to provide detailed information on the composition of the outermost 10 nm surface of the HA nanoshells needed to attribute biological effects to the HA coat. Utilization of isogenic CD44-deficient ($CD44^-$) and CD44-expressing ($CD44^+$) MCF-7 breast cancer cells enabled us to clearly distinguish between unspecific and CD44-mediated uptake and, thereby, simultaneously and robustly determine stealth properties and redirection of the targeting specificity to CD44, the receptor of interest for delivery. We found that coatings created with 33, 260 and 900 kDa HA polymers were effective for decreasing unspecific interaction with $CD44^-$ cells, whereas only 260 and 900 kDa HA nanoshells displayed specific particle retargeting to $CD44^+$ cells, that identifies these polymers for retargeting capability.

Polystyrene particles are inherently hydrophobic and will, therefore, aggregate in water unless sufficiently sterically or electrostatically stabilized (Fig. 4) (25). HA is a hydrophilic polymer made up of disaccharide units containing negatively charged D-glucuronic acid residues at physiologic pH (11), and as a surface coating it, therefore, should constitute both steric and charge stabilization against particle aggregation. Polystyrene particles with a defined core size and uniform number of surface groups for HA attachment allowed any

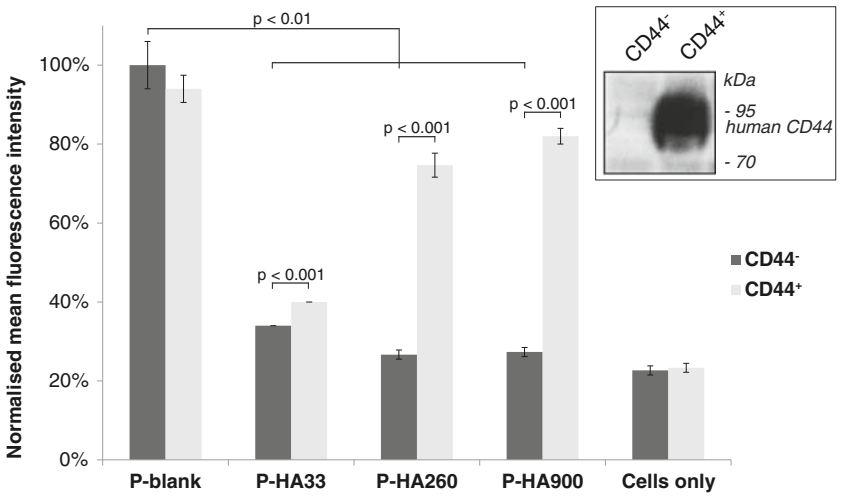


**Fig. 6** Particle uptake in the CD44$^{+/-}$ MCF-7 cell lines based on cellular associated fluorescence. Fluorescent particles were added to cells and incubated for 24 h, the cells where then washed twice and removed. Flow cytometry was performed to evaluate the level of particle uptake based on the geometric mean fluorescence intensity of three replicates. Averages were normalized to cells treated with non-coated particles (P-blank). Insert shows human CD44 antibody stained Western blot of CD44$^{+/-}$ MCF-7 cells – see supporting online information, Figure S3. Statistical significance was evaluated by Students *t*-test.

observed differences to be attributed to the HA material and coating properties.

XPS analysis, in combination with zeta potential measurements was utilized in this study for detailed surface characterization to identify and quantify the HA polymer coating needed to investigate effects of different HA Mw. This is absent in most reported studies that commonly use zeta potential as the only characterization method (21,26,27). XPS analysis confirmed the presence and identity of HA on the particle surfaces as the composition profile change from P-blank (Fig. 3a and Table Ia) to P-HA900 (Fig. 3b and Table Ib) was shifted towards that of the pure HA polymer (Table Ia). The cross sectional area of HA in aqueous solution can be estimated from the radius of gyration, $Rg$ =1.3 nm x Mw(kDa)$^{0.6}$ (12,28) to 90, 1,050 and 4,660 nm$^2$ for the 33, 260 and 900 kDa HA, respectively. Covering more than the area of one surface amine (69 nm$^2$) and comprising several carboxylic acid groups along the chain, one HA polymer could possibly multivalent bind and occupy several surface amines to adopt a flattened surface architecture (Fig. 9a). Increase of HA coating Mw would, in such an arrangement, result in a constant or only slightly increasing overall HA surface mass that would be reflected in the carboxylic acid XPS C1s component. To attach each HA molecule to fewest possible amine groups on average and consequently obtain flexible and non-constricted HA polymers on the particle surface (Fig. 9b), HA was added with excess carboxyl groups (RCOOH: $RNH_2$ ratio was minimum 88:1) and HA polymer

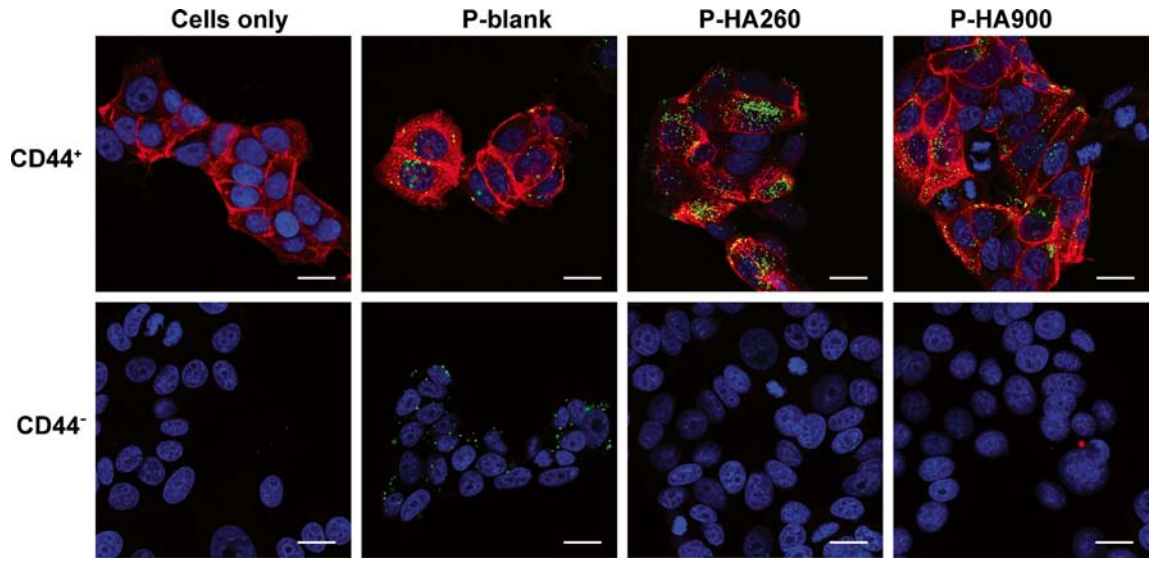


**Fig. 7** Confocal laser scanning microscopy images of MCF-7 (CD44$^{+/-}$) cellular uptake of particles without coating or with HA nanoshells of 260 and 900 kDa. Particles are labeled green (yellow-green), cell nuclei were stained blue (*Hoechst*) and CD44 receptors red (Alexa 647). Scalebar is 2 $\mu$m.

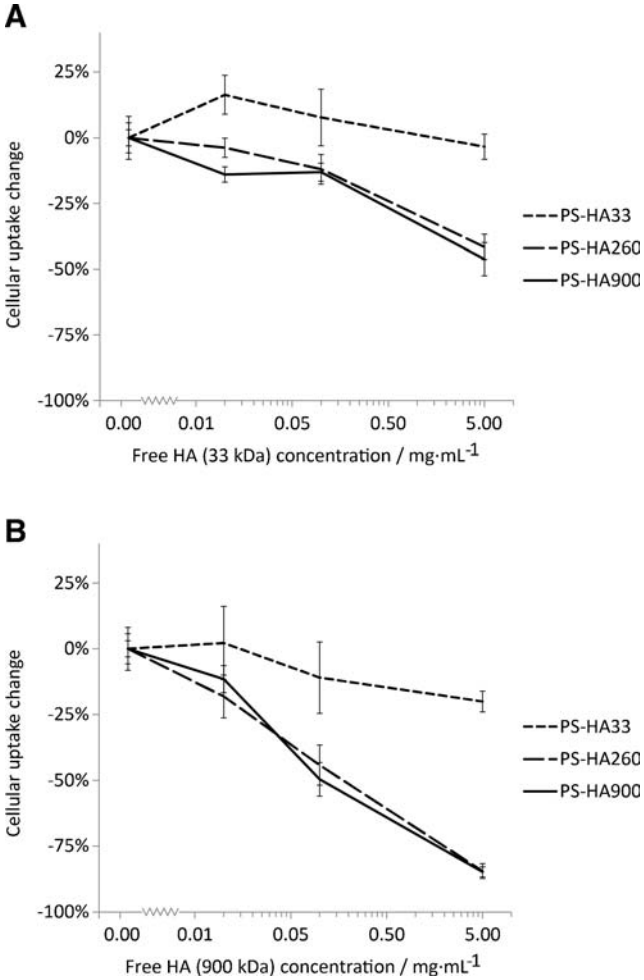


**Fig. 8** Competitive CD44 binding analysis after free HA pre-incubation. MCF-7 ($CD44^+$) cells were pre-incubated for 1 h with free HA of 33 kDa (**a**) and 900 kDa (**b**) (0.0 to 5 mg/mL range) before a 3 h incubation with particles grafted with HA nanoshells. The effect of the free HA was analyzed with flow cytometry. The average %-value of cells showing particle uptake was normalized to the %-value for 0.0 mg/mL free HA. Any uptake changes due to free HA were depicted as deviations from 0% (0% change in uptake).

to amine ratio of ~1:1. In this study, the carboxylic acid content for HA nanoshells increased rapidly towards the value of pure HA (7.1%) with increasing HA Mw (1.7%, P-HA33 to 4.7%, P-HA900, Table I) suggesting a low level of multivalent HA grafting with flexible HMw HA chains extending out from the particle surface. In contrast to zeta potential, XPS directly measured the amount of material on the surface, and thus reliably supports the dependency of HA nanoshell dry state thickness on HA Mw. This supports a nanoshell architecture with HMw hydrated HA structures extending away from the surface and available for either steric protection or CD44 interaction (Fig. 9b).

Zeta potential data confirmed the presence of anionic HA polymers on the surface with the surface charge decreasing from−8.7 mV for P-blank down to−36.4,−42.5 and −48.3 mV for P-HA33,−260 and−900, respectively (Table I). Interestingly, for a 0.3% increase of the carboxylic acid XPS C1s component (P-blank to P-HA33), the magnitude increase in surface charge was substantial (from−8.7 to −36.4 mV) demonstrating the effectiveness of even the 33 kDa HA nanoshells to control the colloidal properties and stability of the nanoparticles.

NTA data (Fig. 4) indicated increased colloidal stability of HA coated particles with reduced hydrodynamic size (200 nm – 350 nm) due to reduced inter-particle aggregation compared to uncoated, inherently hydrophobic, polymer particles (P-blank) that showed a broad size distribution around 600 nm. The conformational size of HA on a surface will be comparable to the radius of gyration, *Rg*, of a HA random coil and adding this to the model particle diameter of 200 nm, the approximation of the hydrodynamic diameters of HA coated particles are 221, 273 and 354 nm for P-HA33,−260 and −900, respectively, which is in agreement with the NTA data (Fig. 4) and the proposed surface architecture (Fig. 9b). Consistently, the presence of HA of increasing Mw on the nanoparticle surface lead to charge stabilization with increasingly negative zeta potentials of−36 to−48 mV compared to −9 mV for non-coated particles (Table I). Particle dispersions are typically stable outside the zeta potential interval +30 mV and−30 mV (29), and HA nanoshells, thus, demonstrated a good ability for conferring not only steric but also electrostatic stability to particles.

SEM analysis revealed uniform particles of 200 nm size (Fig. 5). In the dry state HA nanoshells were not directly visible, however, the coating influenced inter-particle organization such as described by Lin *et al.* (30). Steric and electrostatic repulsion between 900 kDa HA coated particles during the drying phase (Fig. 5d) allowed for enhanced particle rearrangement and packing comparable to colloid crystals (31) as sketched in Fig. 5f. This effect was less evident for P-blank, P-HA33 and P-HA260 (Fig. 5a, b and c, respectively), with aggregation seemingly more diffusion-limited and less ordered (Fig. 5e). Formation of colloidal crystals is a good indicator of coating uniformity and particle dispersability (32), which suggests that especially HMw HA is well suited for particle coatings and could have a novel utilization in colloidal crystal applications (33).

Due to the flexibility and hydrogen bonding capacity of HA, it can coordinate up to a 1,000 times its weight in water (34) and consequently occupy a large volume. In conjunction with negative charge provided from the carboxyl moieties, the material can provide both a steric and an electrostatic barrier for unspecific interactions with the nanoparticle surface. Particle uptake by $CD44^-$ MCF-7 cells (Fig. 6) was significantly reduced (66% −73%, $p<0.01$) with HA nanoshells and showed no major differences for different coating types, suggesting coatings with 33 kDa HA to be virtually as efficient as those with 260 kDa and 900 kDa HA for reducing unspecific cellular interaction. HA shielding for MPS evasion has been previously demonstrated for naturally occurring HMw HA

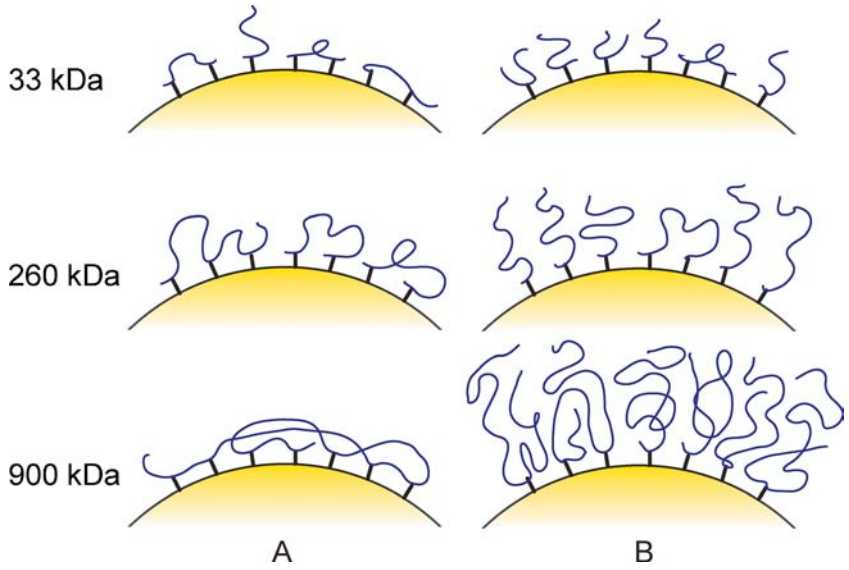


**Fig. 9** Schematic presentation showing the possible arrangements of HA grafted to particle surface amines. Multivalent HA grafting (**a**) leads to a restricted and flattened HA architecture whereas primarily monovalent grafting (**b**) leads to HMw HA structures extending away from the surface available for steric protection and CD44 interaction.

(~1MDa) (26) but to our knowledge not for 33 and 260 kDa HA used in our work. Most existing studies have focused on HA coated liposomes (21,22,35), rather than relatively hydrophobic particles as presented in this work that may reflect inherent differences in cellular interactions between the systems.

HA of various sizes exert its function through binding to one or several cellular surface hyaladherin receptors such as CD44, LYVE-1 or CD168 (RHAMM) (19,20,36). The most studied hyaladherin, CD44, is a type I transmembrane glycoprotein encompassing the highly conserved lectin-like fold, termed the Link module, in the N-terminal HA binding domain (28). By precise arrangement of HA in the CD44 binding site, its features are recognized through hydrogen bonds and van der Waals interactions and binding occurs (37). CD44 is upregulated in a range of human cancers (17,18) and, therefore, constitutes a therapeutic target for HA functionalized nanomedicines. The influence of the CD44 receptor on cellular interaction with HA nanoshells was investigated for the first time in this study using isogenic $CD44^-$ or $CD44^+$ MCF-7 breast cancer cell lines rather than different cell types as previously reported (21,35) that may be influenced by inherent cell-specific differences or by differential expression of HA receptors other than CD44. A study by Mizrahy *et al.* (12) compared the effect of HA Mw (6.4 kDa – 1.5 MDa) on the interaction between HA-modified liposomes and CD44 receptors immobilized on a planar surface. The 2-dimensional planar system, however, does not exactly mimic the 3-dimensional processes involved in cellular recognition and internalization of particles and the influence of membrane fluidity, serum- and cellular membrane proteins utilized in our approach.

The use of isogenic cell lines with and without the CD44 receptor demonstrated CD44-mediated cellular interaction and internalization of P-HA260 and P-HA900 with ~3 times higher fluorescence intensity in $CD44^+$ compared to $CD44^-$ MCF-7 cells (Figs. 6 and 7). CD44 receptor interaction has been reported to occur for HA polymers from 1 – 2 kDa, dependent on the CD44 presenting cell type (12,38), with the interaction strength increasing rapidly with the Mw of HA and HA receptor interactions. However, according to SPR analysis on the CD44-HA interaction, stable and irreversible binding will only occur for free chains in solution at or above a HA size threshold of 30 kDa, independent on CD44 receptor density (28). In our study, 33 kDa HA grafted to particles showed only slightly (6%, $p<0.01$) enhanced particle uptake (Fig. 6). One possible explanation is that attachment of HA to any particle surface results in the immobilized 33 kDa HA being less accessible or flexible compared to free polymer, and thus, less capable of irreversible CD44 binding, but still able to shield the surface from unspecific cellular interaction. In contrast, surface bound HA polymers of 260 or 900 kDa first provides a higher amount of surface HA and, secondly, are sufficiently large and flexible (Fig. 9b) for a high number of CD44 interactions to occur and, therefore, available for strong cellular interaction. As the nanoshells consist of several HA molecules, the number of possible HA-CD44 interactions will increase with higher graft density of the HA molecules, which was one of the reasons for investigating the Mw dependence using a model particle system with a fixed number of surface reactive (amine) groups.

The effect on uptake after pre-incubation with 33 and 900 kDa free HA was investigated to further elucidate the contribution of the CD44-HA binding to the cellular uptake of the HA grafted particles (Fig. 8). The particle uptake of PS-HA33 nanoshells was only slightly reduced by 900 kDa free HA (-20%, $p<0.01$) (Fig. 8b) and not by 33 kDa free HA (Fig. 8a) that confirms that 33 kDa HA only plays a minor role

in CD44 engagement for the polystyrene particle coated system. In contrast, the cellular uptake of PS-HA260 and PS-HA900 was significantly reduced by free 33 kDa HA (up to 42% and 46%, $p < 0.01$) (Fig. 8a) similar to the study of Upadhyay *et al.* using HA-modified polymersomes (39). An almost complete reduction of uptake was observed for 900 kDa free HA (up to 85%, $p < 0.01$) (Fig. 8b). Together, these findings confirm the major and specific contribution of CD44-HA binding to cell uptake of the 260 kDa and 900 kDa surface grafted HA.

P-HA260 and P-HA900 nanoshells promoted internalization of coated particles in $CD44^+$ cells as shown in Fig. 7. It has previously been shown that internalization and degradation is more rapid with HMw (~2 MDa) HA and with a high number of CD44 receptors (40), that is consistent with HA Mw dependent binding strength and the observed internalization in Fig. 7.

Collectively, this work demonstrates the ability of HA nanoshells to confer both shielding of particles from unspecific cellular interactions and specific retargeting by engagement with CD44-presenting cells to mediate binding and uptake through the CD44 receptor. Furthermore, by choosing an appropriate HA Mw, the dual property of HA nanoshells can be tuned according to the desired focus of the application.

## CONCLUSION

Hydrophilic "stealth" coatings can improve biocompatibility of drug delivery nanoparticles and reduce unspecific uptake, but can also compromise retargeting due to ligand enshrouding, consequently a better balance between stealth and targeting is needed. HA is an attractive material for installing dual capacity HA nanoshells to facilitate either stealth properties alone or stealth and targeting due to its physical and molecular properties. In this work we have directly demonstrated the dual property of HA nanoshells to coat, stabilize and protect particles from unspecific cellular interaction and to retarget the coated particles selectively to CD44-expressing cells by modulating the HA molecular weight that can be used in the design of nanoparticle-based nanomedicines.

## ACKNOWLEDGMENTS AND DISCLOSURES

This work was supported by the Lundbeck Foundation grant for the Nanomedicine Center for Individualised Management of Tissue Damage and Regeneration (LUNA), the Lundbeckfonden grant for the Center of Excellence NanoCAN, the EU-FP7-funded NanoAthero project, and co-financed by the INTERREG 4 A-program Syddanmark-Schleswig-K.E.R.N. with funds from The European Regional Development Fund.

## REFERENCES

1. Barenholz Y. Doxil (R) - The first FDA-approved nano-drug: Lessons learned. J Control Release. 2012;160:117–34.
2. Davis ME. The First Targeted Delivery of siRNA in Humans via a Self-Assembling, Cyclodextrin Polymer-Based Nanoparticle: From Concept to Clinic. Mol Pharm. 2009;6:659–68.
3. Owens DE, Peppas NA. Opsonization, biodistribution, and pharmacokinetics of polymeric nanoparticles. Int J Pharm. 2006;307:93–102.
4. Kozlova D, Epple M. Biological targeting with nanoparticles: state of the art. Bio Nano Materials. 2013;14:161–70.
5. Ebbesen M, Whitehead B, Ballarin-Gonzalez B, Kingshott P, Howard K. Surface analysis of PEGylated nano-shields on nanoparticles installed by hydrophobic anchors. Pharm Res. 2013;30:1758–67.
6. Garay RP, El-Gewely R, Armstrong JK, Garratty G, Richette P. Antibodies against polyethylene glycol in healthy subjects and in patients treated with PEG-conjugated agents. Expert Opinion on Drug Delivery. 2012;9:1319–23.
7. Schellekens H, Hennink WE, Brinks V. The immunogenicity of polyethylene glycol: facts and fiction. Pharm Res. 2013;30:1729–34.
8. Hamad I, Hunter AC, Szebeni J, Moghimi SM. Poly(ethylene glycol)s generate complement activation products in human serum through increased alternative pathway turnover and a MASP-2-dependent process. Mol Immunol. 2008;46:225–32.
9. Knop K, Hoogenboom R, Fischer D, Schubert US. Poly(ethylene glycol) in Drug Delivery: Pros and Cons as Well as Potential Alternatives. Angew Chem Int Ed. 2010;49:6288–308.
10. Gabizon AA, Shmeeda H, Zalipsky S. Pros and cons of the liposome platform in cancer drug targeting*. J Liposome Res. 2006;16:175–83.
11. Pouyani T, Prestwich GD. Functionalized Derivatives of Hyaluronic Acid Oligosaccharides: Drug Carriers and Novel Biomaterials. Bioconjug Chem. 1994;5:339–47.
12. Mizrahy S, Raz SR, Hasgaard M, Liu H, Soffer-Tsur N, Cohen K, *et al.* Hyaluronan-coated nanoparticles: The influence of the molecular weight on CD44-hyaluronan interactions and on the immune response. J Control Release. 2011;156:231–8.
13. Day AJ, Sheehan JK. Hyaluronan: polysaccharide chaos to protein organisation. Curr Opin Struct Biol. 2001;11:617–22.
14. Peer D, Park EJ, Morishita Y, Carman CV, Shimaoka M. Systemic leukocyte-directed siRNA delivery revealing cyclin D1 as an anti-inflammatory target. Science. 2008;319:627–30.
15. Naor D, Nedvetzki S, Golan I, Melnik L, Faitelson Y. CD44 in Cancer. Crit Rev Clin Lab Sci. 2002;39:527–79.
16. Bartolazzi A, Peach R, Aruffo A, Stamenkovic I. Interaction between CD44 and hyaluronate is directly implicated in the regulation of tumor development. J Exp Med. 1994;180:53–66.
17. Shigeishi H, Fujimoto S, Hiraoka M, Ono S, Taki M, Ohta K, *et al.* Overexpression of the receptor for hyaluronan-mediated motility, correlates with expression of microtubule-associated protein in human oral squamous cell carcinomas. Int J Oncol. 2009;34:1565–71.
18. Mohapatra S, Yang XW, Wright JA, Turley EA, Greenberg AH. Soluble hyaluronan receptor RHAMM induces mitotic arrest by suppressing Cdc2 and cyclin B1 expression. J Exp Med. 1996;183:1663–8.
19. Fraser J, Laurent T, Laurent U. Hyaluronan: its nature, distribution, functions and turnover. J Intern Med. 1997;242:27–33.

20. Platt VM, Szoka Jr FC. Anticancer therapeutics: Targeting macromolecules and nanocarriers to hyaluronan or CD44, a hyaluronan receptor. Mol Pharm. 2008;5:474–86.
21. Eliaz RE, Nir S, Szoka FC. Interactions of hyaluronan-targeted liposomes with cultured cells: Modeling of binding and endocytosis. Liposomes, Pt D. 2004;387:16–33.
22. Qhattal HSS, Liu X. Characterization of CD44-Mediated Cancer Cell Uptake and Intracellular Distribution of Hyaluronan-Grafted Liposomes. Mol Pharm. 2011;8:1233–46.
23. Almalik A, Karimi S, Ouasti S, Donno R, Wandrey C, Day PJ, *et al.* Hyaluronic acid (HA) presentation as a tool to modulate and control the receptor-mediated uptake of HA-coated nanoparticles. Biomaterials. 2013;34:5369–80.
24. Tømmeraas K, Melander C. Kinetics of Hyaluronan Hydrolysis in Acidic Solution at Various pH Values. Biomacromolecules. 2008;9: 1535–40.
25. Binks BP, Lumsdon SO. Pickering Emulsions Stabilized by Monodisperse Latex Particles: Effects of Particle Size. Langmuir. 2001;17:4540–7.
26. Peer D, Margalit R. Tumor-targeted hyaluronan nanoliposomes increase the antitumor activity of liposomal doxorubicin in syngeneic and human xenograft mouse tumor models. Neoplasia. 2004;6:343–53.
27. El-Dakdouki MH, El-Boubbou K, Zhu DC, Huang XF. A simple method for the synthesis of hyaluronic acid coated magnetic nanoparticles for highly efficient cell labelling and in vivo imaging. Rsc Advances. 2011;1:1449–52.
28. Wolny PM, Banerji S, Gounou C, Brisson AR, Day AJ, Jackson DG, *et al.* Analysis of CD44-Hyaluronan Interactions in an Artificial Membrane System: Insights into the distinct binding properties of high and low molecular weight hyaluronan. J Biol Chem. 2010;285: 30170–80.
29. Israelachvili JN. Intermolecular and surface forces: revised third edition: Academic press. 2011.
30. Lin MY, Lindsay HM, Weitz DA, Ball RC, Klein R, Meakin P. Universality in colloid aggregation. Nature. 1989;339.
31. Goodwin JW. Colloids and Interfaces with Surfactants and Polymers: An Introduction. West Sussex: John Wiley & Sons; 2004.
32. Ohno K, Ma Y, Huang Y, Mori C, Yahata Y, Tsujii Y, *et al.* Surface-Initiated Reversible Addition-Fragmentation Chain Transfer (RAFT) Polymerization from Fine Particles Functionalized with Trithiocarbonates. Macromolecules. 2011;44:8944–53.
33. Mukhopadhyay R, Al-Hanbali O, Pillai S, Hemmersam AG, Meyer RL, Hunter AC, *et al.* Ordering of binary polymeric nanoparticles on hydrophobic surfaces assembled from low volume fraction dispersions. J Am Chem Soc. 2007;129:13390–1.
34. Volný M, Elam WT, Ratner BD. Tureček F. Enhanced in–vitro blood compatibility of 316 L stainless steel surfaces by reactive landing of hyaluronan ions. Journal of Biomedical Materials Research Part B: Applied. Biomaterials. 2007;80:505–10.
35. Eliaz RE, Szoka FC. Liposome-encapsulated doxorubicin targeted to CD44: A strategy to kill CD44-overexpressing tumor cells. Cancer Res. 2001;61:2592–601.
36. Day AJ, Prestwich GD. Hyaluronan-binding proteins: Tying up the giant. J Biol Chem. 2002;277:4585–8.
37. Banerji S, Wright AJ, Noble M, Mahoney DJ, Campbell ID, Day AJ, *et al.* Structures of the Cd44–hyaluronan complex provide insight into a fundamental carbohydrate-protein interaction. Nat Struct Mol Biol. 2007;14:234–9.
38. Stern R, Asari AA, Sugahara KN. Hyaluronan fragments: An information-rich system. Eur J Cell Biol. 2006;85:699–715.
39. Upadhyay KK, Bhatt AN, Mishra AK, Dwarakanath BS, Jain S, Schatz C, *et al.* The intracellular drug delivery and anti tumor activity of doxorubicin loaded poly(gamma-benzyl L-glutamate)-b-hyaluronan polymersomes. Biomaterials. 2010;31:2882–92.
40. Culty M, Nguyen HA, Underhill CB. The hyaluronan receptor (CD44) participates in the uptake and degradation of hyaluronan. J Cell Biol. 1992;116:1055–62.